A scalar Poincaré map for struggling in *Xenopus* tadpoles

Mark Olenik[1], Conor Houghton[2]

Schools of [1]Biological Sciences and [2]Computer Science, University of Bristol, Bristol BS81TH, United Kingdom

Abstract

Synaptic plasticity is widely found in many areas of the central nervous system. In particular, it is believed that synaptic depression can act as a mechanism to allow simple networks to generate a range of different firing patterns. The simplicity of the locomotor circuit in hatchling *Xenopus* tadpoles provides an excellent place to understand such basic neuronal mechanisms. Depending on the nature of the external stimulus, tadpoles can generate two types of behaviours: swimming when touched and slower, stronger struggling movements when held. Struggling is associated with rhythmic bends of the body and is accompanied by anti-phase bursts in neurons on each side of the spinal cord. Bursting in struggling is thought to be governed by a short-term synaptic depression of inhibition. To better understand burst generation in struggling, we study a minimal network of two neurons coupled through depressing inhibitory synapses. Depending on the strength of the synaptic conductance between the two neurons, such a network can produce symmetric $n-n$ anti-phase bursts, where neurons fire n spikes in alternation, with the period of such solutions increasing with the strength of the synaptic conductance. Using a fast/slow analysis, we reduce the multidimensional network equations to a scalar Poincaé burst map. This map tracks the state of synaptic depression from one burst to the next, and captures the complex bursting dynamics of the network. Fixed points of this map are associated with stable burst solutions of the full network model, and are created through fold bifurcations of maps. We prove that the map has an infinite number of stable fixed points for a finite coupling strength interval, suggesting that the full two-cell network also can produce $n-n$ bursts for arbitrarily large n. Our findings further support the hypothesis that synaptic depression can enrich the variety of activity patterns a neuronal network generates.

Keywords: *Xenopus*, Synaptic depression, Poincaré map, Dynamical system

1. Introduction

Short-term synaptic plasticity may have a role in burst activity in central pattern generators (CPGs). Short-term synaptic depression is commonly found in neuronal networks involved in the generation of rhythmic movements, such as in the pyloric CPG of the spiny lobster (Rabbah and Nadim, 2007), or in the lumbosacral cord of the chick embryo (Donovan et al., 1998). Synaptic depression modulates the strength of synapses in response in changes to the presynaptic firing frequency. At a high neuronal firing frequency, depression weakens the strength of synapses and therefore reduces the magnitude of the respective postsynaptic response. At low firing frequency, in contrast, it allows sufficient time for the synapse to recover from depression between spikes, leading to a stronger postsynaptic response. In reciprocal networks, synaptic depression has been shown to act as a "switch", giving rise to a wide range of network dynamics such as synchronous and multi-stable rhythms, as well as fine tuning the frequency of network oscillations (Nadim and Manor, 2000; Nadim et al., 1999; Bose and Booth, 2011).

A switch between two CPG rhythms that is guided by synaptic depression can be observed in hatchling *Xenopus* tadpoles. Tadpoles select between two main behaviours in response to different types of skin stimuli. Swimming occurs in response to a brief touch or a single electrical pulse to the trunk (Clarke et al., 1984), and is accompanied by low-amplitude 12 to 25 Hz alternating left and right bending moves that progress from head to tail (Kahn et al., 1982). Alternatively if held, tadpoles produce struggling, with slower 2 to 10 Hz bending moves of the whole body that spread in the opposite direction, from the tail to the head (Kahn and Roberts, 1982). The switch from swimming to struggling is associated with a change from a pattern of low-frequency alternating single spikes in swimming at $12 - 25$ Hz (Kahn et al., 1982), to one of alternating high-frequency bursting in struggling, with bursts occurring at periods ranging from 100 to 500 ms (Kahn and Roberts, 1982; Soffe, 1993). The synaptic depression substantially weakens synapses and guides the network rhythm during the high-frequency bursts in struggling. Both swimming and struggling are produced by two overlapping spinal cord CPG networks that share some types of individual neurons. One

such shared class of neurons are the inhibitory commissural interneurons (cINs), which have reciprocal depressing inhibitory synapses with neurons on the opposite site of the spinal cord (Li et al., 2007).

It has been proposed that this synaptic depression of reciprocal inhibition can act as a burst termination mechanism during struggling: while one side of the spinal cord is firing, inhibition from cINs prevents the other side from firing. Weakening of inhibition as a result of synaptic depression allows the antagonistic side to be released, start firing, and terminate the ongoing burst. This periodic process is believed to produce the rhythmic anti-phase bursts found in tadpole struggling. Such anti-phase bursty rhythms have been previously replicated in a small half-centre neuronal network model that contains the four main types of neurons active during struggling (Li et al., 2007): ascending interneurons, repetitive firing descending interneurons, motoneurons, and cINs. In this model each neuron population is approximated by three biophysical neurons, so there are 18 cells in the network. In line with Brown's (1911) hypothesis of rhythmogenesis in the spinal cord, the model relies on depression of reciprocal inhibition between cINs to act as a burst termination mechanism. While the model in Li et al. (2007) reproduces the struggling-like burst patterns qualitatively, burst rhythm generation in this model has not been investigated systematically, nor does the model provide a description for how depression controls the network dynamics.

To address these questions we reduce the complexity of the struggling network to a simpler formulation of Brown's (1911) rhythmogenesis hypothesis. We study the mechanisms of burst generation in struggling using a generic half-centre CPG that consists of two identical, tonically active neurons that are coupled through inhibitory depressing synapses. Each neuron represents a population of cINs on either side of the tadpole spinal cord. Our model reduction is based on the approach previously taken by Bose and Booth (2011), where the dynamics of a similar two-cell reciprocal inhibitory network with depression has been analysed. Bose and Booth (2011) relied on the methods from geometric singular perturbation theory to separate the timescales of the fast membrane, and the slow synaptic dynamics of the network to derive one-dimensional conditions for the existence of stable anti-phase burst solutions. While these conditions justify the existence of bursting, they do not explain how such solutions are created nor what shapes their parameter space. Here, we extend the analysis by Bose and Booth (2011) by constructing a scalar Poincareé map which tracks the evolution of depression from one burst to the next, and whose fixed points correspond to stable burst solu-

tions of the two-cell network. Our map construction is motivated by the burst length map of a T-type calcium current, utilised in Matveev et al. (2007), which approximates the anti-phase bursting dynamics of a network of two coupled Morris-Lecar (Morris and Lecar, 1981) neurons. This network does not contain short-term synaptic depression, and burst termination is instead accomplished through the dynamics of a slow T-type calcium current which makes the single cells bursty, even in absence of network interactions.

This paper is organised as follows. First, we introduce the network of two neurons, and describe the properties of the single cell and synapse dynamics. We use numerical simulations of the network to provide an intuition for the range of possible burst dynamics the system can produce. Next, we state the simplifying assumptions and perform a fast-slow analysis of the single cell equations, resulting in an algebraic equation that uniquely determines the type of burst solution a network displays. Then, we analytically derive the first return map of the depression variable, first assuming that solutions consist of n spikes, and later relaxing this assumption. We end this work with a conclusion.

2. Model

2.1. Model Description

For numerical simulations we consider a pair of identical Morris-Lecar neurons (Morris and Lecar, 1981), with parameters adopted from Bose and Booth (2011). The Morris-Lecar model is a set of two first-order differential equations that describe the membrane dynamics of a spiking neuron. The depolarisation is modelled by an instantaneous calcium current, and the hyperpolarisation by a slow potassium current and a leak current. The membrane potential v_i and potassium activation w_i of neuron i $(i, j = 1, 2)$ is described by:

$$\dot{v}_i = f(v_i, w_i) - \bar{g} s_j (v_i - v_s), \tag{1}$$

$$\dot{w}_i = h(v_i, w_i). \tag{2}$$

Here v_s is the inhibitory reversal potential, and $\bar{g}$ and s_j are the maximal synaptic conductance and the synaptic gating, respectively, constituting the total inhibitory conductance $\bar{g} s_j$ from neuron j to neuron i. Function $f(v_i, w_i)$ describes the membrane currents of a cell that include a constant

current I, and three ionic currents: an instantaneous calcium current, a potassium current, and a leak current, with respective reversal potentials v_{Ca}, v_K, and v_L, as well as maximum conductances g_{Ca}, g_K, and g_L:

$$f(v_i, w_i) = -g_{Ca} m_\infty(v_i)(v_i - v_{Ca}) - g_K w_i (v_i - v_K) - g_L(v_i - v_L). \tag{3}$$

The function $h(v_i, w_i)$ models the kinetics of the potassium gating variable w_i, and is given by

$$h(v_i, w_i) = \frac{w_\infty(v_i) - w_i}{\tau_w}. \tag{4}$$

The asymptotic functions m_∞ and w_∞ for the calcium and potassium conductances, respectively, are given by

$$m_\infty(v_i) = \frac{1}{2}\left(1 + \tanh\left((v_i - v_A)/v_B\right)\right), \tag{5}$$

$$w_\infty(v_i) = \frac{1}{2}\left(1 + \tanh\left((v_i - v_C)/v_D\right)\right). \tag{6}$$

All model parameters are given in Table 1.

Our mathematical analysis is performed on the equations of a single cell, which is why we will omit the subscripts i, j from here on. When the cells are uncoupled ($\bar{g} = 0$), the membrane dynamics are determined by the cubic v-nullcline ($v_\infty(v)$ with

$$v_\infty(v) = \frac{-g_{ca} m_\infty(v)(v - v_{ca}) - g_l(v - v_l) + I}{g_K(v - v_k)}, \tag{7}$$

and the sigmoid w-nullcline $w_\infty(v)$, satisfying $\dot{v} = 0$ and $\dot{w} = 0$, respectively. The two curves intersect along the middle branch of v_∞, creating an unstable fixed point p_f with a surrounding stable limit cycle of period T (Figure 1A). Trajectories along that limit cycle have the familiar shape of the action potential (Figure 1B). The trajectory of an action potential can be dissected into four phases: (1) a silent phase, (2) a jump up, (3) an active phase, and (4) a jump down (see e.g. Ermentrout and Terman, 2010). During the silent phase the trajectory evolves along the left branch ($v < v_\theta$) of the cubic v-nullcline. Once the trajectory reaches the local minimum of v_∞ at (v_L, w_L), it "jumps up" to the right branch, crossing the firing threshold v_θ. During

Table 1: Parameter for coupled Morris-Lecar model.

Parameter	value
g_l	0.15 mS/cm^2
g_{Ca}	0.3 mS/cm^2
g_K	0.6 mS/cm^2
v_K	-70 mV
v_L	-50 mV
v_{Ca}	100 mV
v_A	1 mV
v_B	14.5 mV
v_C	4 mV
v_D	15 mV
I	6 μA/cm^2
τ_w	100 ms
τ_d	1000 ms
τ_s	100 ms
v_θ	0 mV
v_s	-80 mV
λ	0.5
T	217 ms

the active phase the trajectory then evolves along the right branch of the cubic until it arrives at the local maximum (v_R, w_R), where it "jumps down" to the left branch.

Applying a constant inhibitory conductance $\bar{g}s > 0$ moves the cubic v_∞ with the ensuing unstable fixed point down the sigmoid w_∞ in the $(v - w)$-plane. When the synaptic conductance $\bar{g}s$ is large enough, p_f becomes stable and all periodic trajectories relax into an equilibrium (see Figure 2). There exists a unique value $\bar{g}s = g^\star$ when the fixed point lies exactly on the left local minimum of v_∞. This is where the fixed point changes stability via a sub-critical Andronov-Hopf bifurcation and the stable limit cycle vanishes via a fold bifurcation of limit cycles (e.g. see Ermentrout and Terman, 2010). Thus, when a constant inhibitory conductance is applied, $g^\star$ acts as a *release conductance*: a cell is prevented from tonic spiking when $\bar{g}s > g^\star$ and it will fire spikes when $\bar{g}s < g^\star$ (Bose and Booth, 2011).

The dynamics of the synaptic interactions between the neurons is gov-

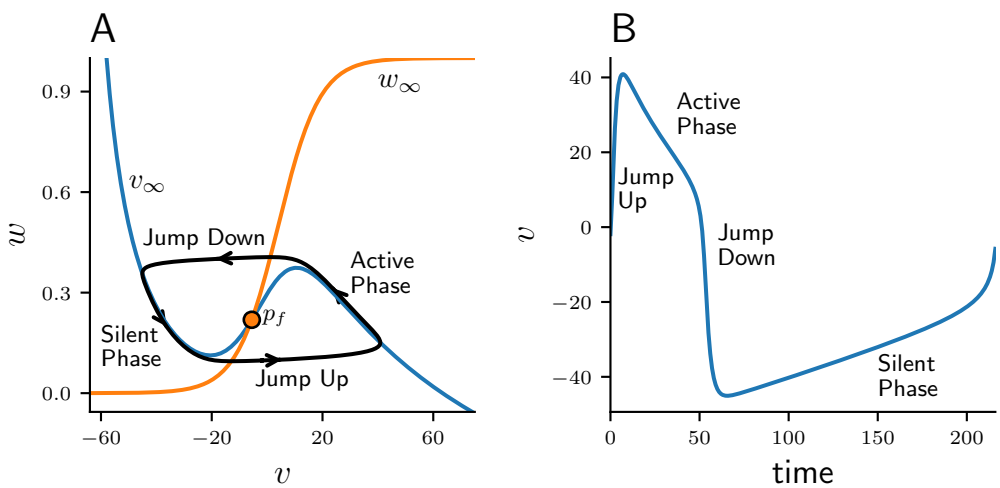

Figure 1: Periodic solution of relaxation-oscillator model neuron. **A**: Projection of limit cycle onto (v, w)-phase plane with v-nullcline (blue, v_∞) and w-nullcline (orange, w_∞). Unstable fixed point p_f is indicated by an orange dot. **B**: Corresponding voltage trace of an action potential.

erned by a synaptic gating variable s, and a depression variable d.

$$\dot{s} = -s/\tau_s, \tag{8}$$

$$\dot{d} = (1-d)/\tau_d. \tag{9}$$

Variable d describes a firing rate dependent depletion mechanism that governs the amount of depression acting on the synapse; our model is agnostic with respect to the exact mechanism of this depletion, be it pre- or post-synaptic. At spike time when the voltage v crosses a synaptic threshold v_θ, the synaptic gating variable s is reset to the current value of the depression variable d, and d is scaled down by the depression strength parameter λ $(0 < \lambda < 1)$. This results in the following discontinuous reset rule on spike time:

$$s \leftarrow d, \tag{10}$$

$$d \leftarrow \lambda d. \tag{11}$$

The equations for the depression model were adapted from Bose et al. (2001). These equations are a mathematically tractable simplification of the estab-

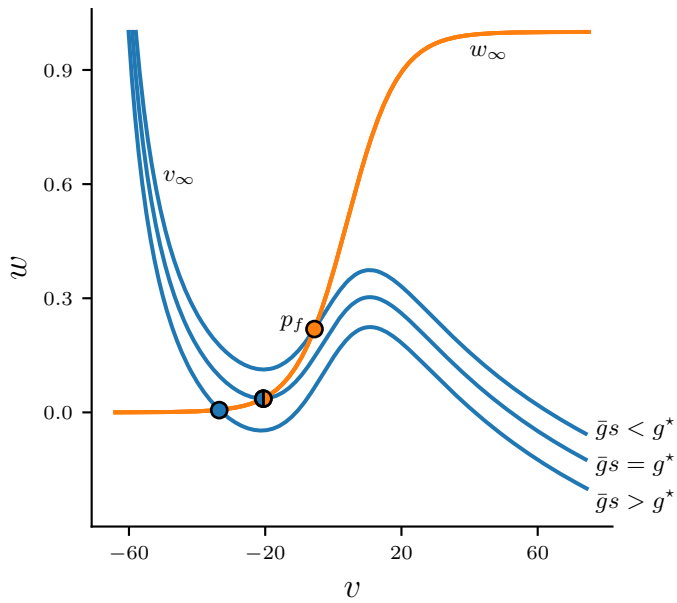

Figure 2: Nullclines v_∞ (blue) and w_∞ (orange) in (v, w)-phase plane for different values of the total synaptic conductance $\bar{g}s$. For small $\bar{g}s < g^\star$, fixed point p_f is unstable (orange point). Larger values of $\bar{g}s$ move v_∞ down in the (v, w)-plane until p_f changes stability (half orange, half blue point) at some critical total conductance value $\bar{g}s = g^\star$, and becomes stable (blue point) for $\bar{g}_{g^\star}$.

lished phenomenological depression model previously described by Tsodyks and Markram (1997). The original equations in Bose et al. (2001) include an exponential decay of d throughout the active phase of the action potential, that is

$$\dot{d} = -d/\tau_\beta, \tag{12}$$

while $v > v_\theta$ for a decay time constant τ_β. To simplify the mathematical analysis we have reduced these dynamics to a single-reset event at spike time according to (11). It is easy to see that this simplification is natural given a constant duration of the active phase of an action potential, and it will become evident from our results that this simplification does not qualitatively change the dynamics of the network compared to the original equations with depression dynamics described by (12).

2.1.1. Anti-Phase Bursting Solutions

Short-term synaptic depression of inhibition in a half-centre oscillator acts as a *burst termination* mechanism and is known to produce $n-n$ anti-phase burst solutions of varying period. Such $n-n$ solutions consist of cells firing bursts of n spikes in alternation (see Figure 3A). While one cell is firing a burst it provides an inhibitory conductance to the other cell thus preventing it from firing. Therefore, at any given moment one cell is spiking while the other is inhibited. Consistent with Bose and Booth (2011) we will refer to the currently firing cell as "free" and we will call the inhibited cell "quiet". Additionally, we will distinguish between two phases of a $n-n$ solution: We will refer to the burst duration of a cell as the "free phase", and we will call the remaining duration of a cycle, when a cell is not spiking, the "quiet phase".

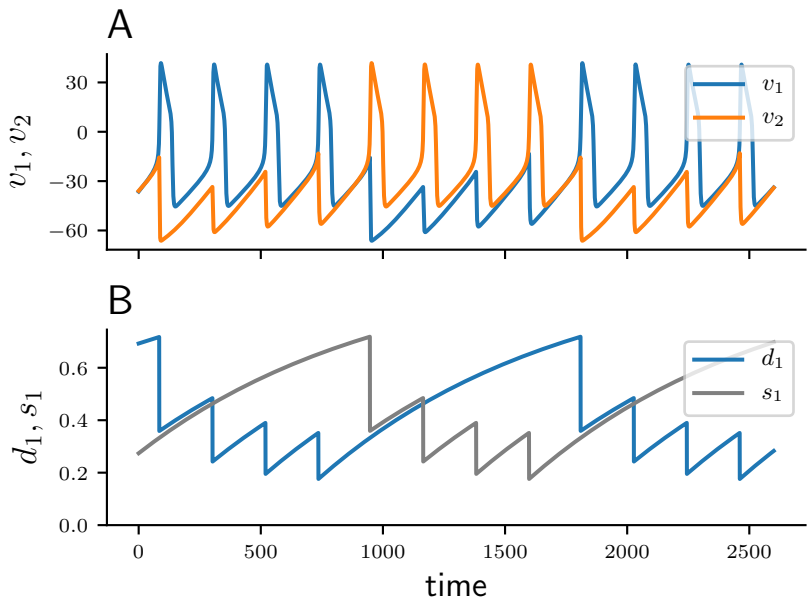

Figure 3: Solution profiles of a $4-4$ burst. **A**: Membrane potentials of cell 1 (v_1, blue), and cell 2 (v_2, orange). **B**: Synaptic variables d_1 (blue) and s_1 (grey) of cell 1.

With each action potential of the free cell, short-term depression leads to a step-wise decrease of d, and consequently of s. If d depresses faster at spike time than it can recover in the inter-spike-intervals (ISIs), the total synaptic conductance $\bar{g}s$ will eventually become sufficiently small to allow the quiet

cell to be released and start firing, thus inhibiting the previously free cell. While a cell is quiet its associated depression variable can recover. Once the quiet cell is released its inhibition will be sufficient to terminate the burst of the previously free cell and commence a new cycle. Figure 3B depicts the depression and recovery of d as well as the discontinuous resets of s in a $4-4$ burst.

As previously demonstrated by Bose and Booth (2011), the coupling strength $\bar{g}$ plays a crucial role in the generation of burst solutions in a two-cell reciprocally inhibitory network with synaptic depression. In particular, they found that increasing $\bar{g}$ produces longer $n-n$ bursts. Figure 4 shows numerically stable $n-n$ solutions for varying values of $\bar{g}$. For small values of $\bar{g}$ the network produces anti-phase spiking $(1-1)$. As $\bar{g}$ is increased the network generates solutions of increasing n, that is $2-2$, $3-3$, and so on. When the coupling strength $\bar{g}$ is sufficiently large, that is $\bar{g} > \bar{g}_{sup} \approx 1.016$ mS/cm^2, (bottom of Figure 4), one of the cells continuously spikes at its uncoupled period T while the other cell is fully suppressed.

We numerically compute the bifurcation diagram of stable $n-n$ solutions with the control parameter $\bar{g}$ (see Appendix for algorithm description). Figure 5A depicts the period P of $n-n$ solutions as $\bar{g}$ is varied. Stable $n-n$ solutions have a period that lies some interval $(2(n-1)T, 2nT)$. Therefore, $n-n$ solutions are created at some period $P > 2(n-1)T$ and destroyed at exactly $P = 2nT$. Moreover, stable $n-n$ solutions of longer period occur on increasingly smaller intervals of $\bar{g}$. In particular, large period $n-n$ solutions exist between the $5-5$ and the suppressed solutions (region between dotted lines in Figure 5A, solution branches not displayed).

2.2. Mathematical Analysis of Two-Cell Network

The goal of the following mathematical analysis will be to reduce the complexity of the eight-dimensional system to some easily tractable quantity. As we will see later this quantity is the value of the depression variable d of one of the two cells. We will then construct the evolution of d for the free and quiet phases of the cycle separately. Having a description of the full cycle in terms of d will allow us to explore the parameter space and understand *how* these $n-n$ burst solutions are created. The main arguments in the following two sub-sections 2.2.1 and 2.2.2 were first explored in Bose and Booth (2011) and will be explained in more detail below. However, while Bose and Booth (2011) used these arguments to derive algebraic conditions that guarantee the periodicity of the depression variable for different $n-n$ solutions, we will

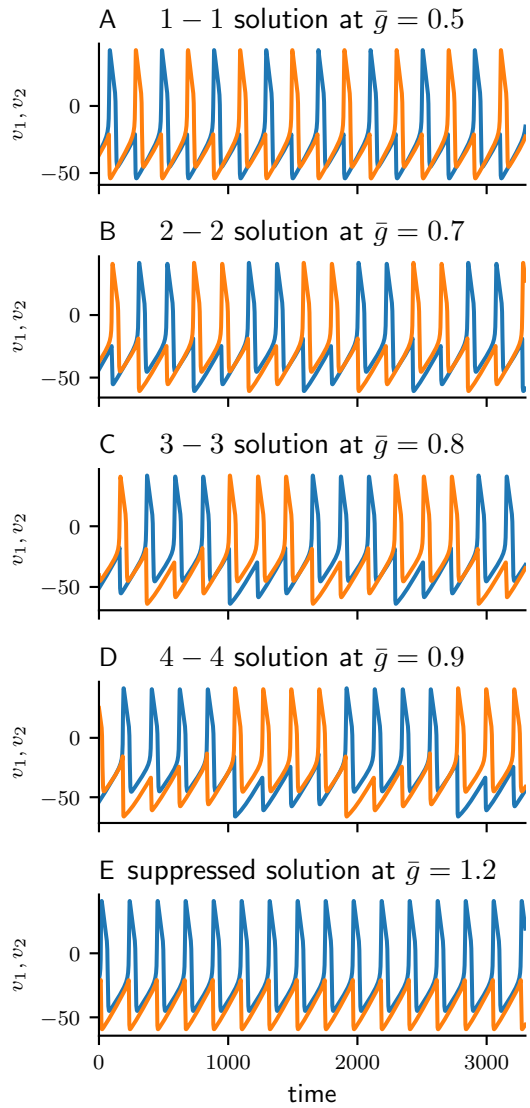

Figure 4: Stable $n-n$ solutions for increasing values of the coupling strength $\bar{g}$ (increasing top to bottom).

use these arguments to construct a Poincaré map of d, which will provide an intuition for the dynamics of d.

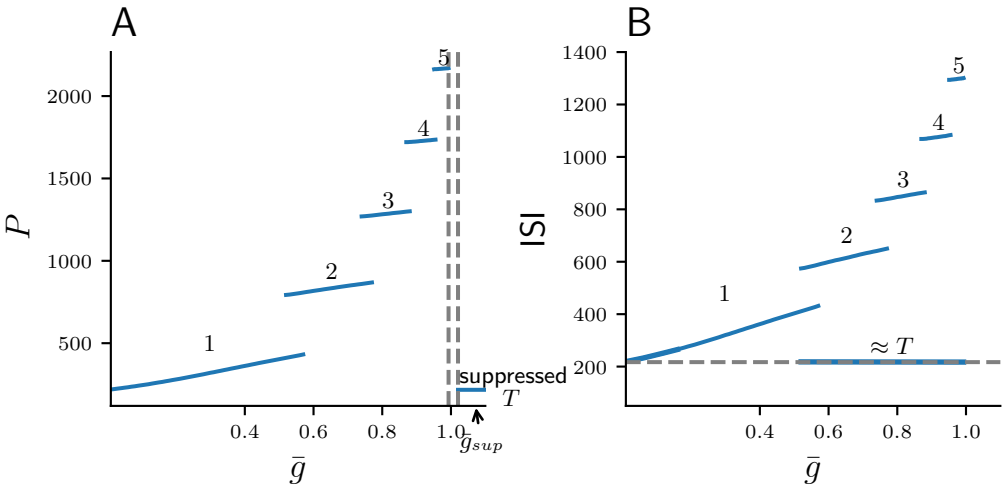

Figure 5: Numerically computed bifurcation diagrams of stable $n-n$ solutions for increasing coupling strength $\bar{g}$. **A**: Period P of stable solutions. Dashed lines show the interval between the $5-5$ and the suppressed solutions, where higher period $n-n$ solutions occur on increasingly smaller ranges of $\bar{g}$. **B**: ISIs corresponding to $n-n$ solutions in A. Long ISIs are associated with the quiet phase of a burst, short ISIs with the free phase. During the free phase, ISIs are of approximately constant duration T.

2.2.1. Assumption ISI=T

The following mathematical analysis is greatly simplified by assuming that the ISIs during the free phase are of constant duration T. That is to say, once a cell becomes free, it fires at its uncoupled period T. This assumption seems reasonable given that (1) the inhibitory conductance decays exponentially to zero during the quiet phase of a cycle, and (2) the fact that many biophysical neuron models, such as the Morris-Lecar model, will fire at approximately their uncoupled period T once released from inhibition.

It is evident from the burst solutions presented in Figure 4 that the respective ISIs in the free phase are nearly constant. We further verify this observation by computing the associated ISIs of stable solutions found in Figure 5A. Figure 5B illustrates the bifurcation diagram of ISIs for varying $\bar{g}$. Naturally, burst solutions with $n > 1$ contain two types of ISIs: Long ISIs during the quiet phase, and short ISIs in the free phase. Note that in the latter ISIs are nearly constant, $ISI \approx T$, affirming the above assumption. The assumption $ISI = T$ allows us to ignore the membrane dynamics of the free cell, and construct the evolution of its synaptic variables iteratively from

spike to spike. By tracking the exact values of d and s of the free cell we will determine when the quiet cell is released and becomes free, terminating the burst of the previously free cell. In the next section we will define such a "release condition" by exploiting the discrepancy in timescales between the fast voltage dynamics, and the slow potassium and synaptic dynamics.

2.2.2. Fast/Slow Analysis of Single Cell Model

Neuronal membrane dynamics typically involve mechanisms that evolve on very different timescales. In the case of a single Morris-Lecar neuron (Figure 1) the trajectory spends a lot of time in the silent and active phases, while the voltage jumps up and down occur seemingly instantaneously. Geometric singular perturbation theory provides methods to utilise such discrepancy in timescales (Fenichel, 1979). Consider equations (1) and (2) for an uncoupled Morris-Lecar neuron with $\bar{g} = 0$. By rescaling $f = \tilde{f}/\epsilon$ we obtain the generic equations of a fast/slow system:

$$\epsilon \dot{v}_i = \tilde{f}(v_i, w_i), \tag{13}$$

$$\dot{w}_i = h(v_i, w_i). \tag{14}$$

By analysing these equations in the limit $\epsilon \to 0$, we will find an explicit description of the action potential that is of a lower dimension than the original system. Consider two timescales: a slow timescale t that describes the evolution of v and w in the silent and active phases, and a fast timescale τ that is used to describe the jumps up and down. We initially inspect the fast timescale τ: By first substituting $t = \epsilon\tau$, and then setting $\epsilon = 0$ we acquire the singularly perturbed system of equations

$$v' = \tilde{f}(v, w), \tag{15}$$

$$w' = 0. \tag{16}$$

Here the prime symbol "$\prime$" represents the derivative with respect to τ. The first equation describes the evolution of the voltage as $t \to \infty$ during the up- and down jumps, that is from the local extrema (v_L, w_L) and (v_R, w_R) respectively to the opposite branch. The second equation implies that during those jumps the slow variable w is constant. For the jump up we have $w = w_L$ while for the jump down $w = w_R$. In the singular limit we can therefore simplify the jump dynamics to the scalar equation:

$$v' = \tilde{f}(v, w_{L,R}). \tag{17}$$

Now, consider the slow timescale t by setting $\epsilon = 0$:

$$0 = \tilde{f}(v, w), \tag{18}$$

$$\dot{w} = h(v, w). \tag{19}$$

The first equation describes the v-nullcline and the second equation models the evolution of the slow variable w along the left and right branches of that v-nullcline during the silent and active phases respectively. Here we can use the implicit function theorem to express this evolution of w as a scalar equation by replacing v with its associated asymptotic value. Let $v_L(w)$ and $v_R(w)$ describe the v-nullcline on the left and right branches, that is for $v < v_L$ and $v > v_R$ respectively. Then the slow timescale dynamics are given by:

$$\dot{w} = h\left(v_{L,R}(w), w\right). \tag{20}$$

In sum, geometric singular perturbation theory allows us to reduce the two-dimensional uncoupled Morris-Lecar model to two scalar differential equations for the fast and slow phases of an action potential respectively, at least in the limit $\epsilon \to 0$. In the above analysis we assumed *uncoupled* cells, that is $\bar{g} = 0$. In the following section we will extend the analysis to include synaptic interaction in the network when $\bar{g} > 0$.

2.2.3. Release Condition

Our assumption for the free cell states that it fires at its uncoupled period ($ISI = T$). We can therefore disregard weak inhibition ($\bar{g}s < g^\star$) in our analysis. Instead, we concentrate on the dynamics of the quiet cell under strong inhibition, when $\bar{g}s - g^\star$ is sufficiently large. In this case, the v- and w-nullclines intersect to the left of v_L creating a stable fixed point p_f at some (v_{p_f}, w_{p_f}) (Figure 2). Each time the free cell produces a spike, p_f jumps down along the w-nullcline and becomes stable. The inhibitory conductance $\bar{g}s$ then decays exponentially according to equation (8), and p_f moves back up the $(v - w)$-plane. For $\bar{g}$ sufficiently large, our previous fast-slow analysis can be extended to include these piecewise-continuous synaptic dynamics.

Our singular equations for the fast system predict that v will be at its equilibrium value of v_{p_f} immediately after the pre-synaptic spike and will remain at the fixed point as the v-nullcline moves. What about w? If the change in w-direction is significantly faster than the change in s direction, w will quickly approach w_{p_f} after the pre-synaptic spike. As the synaptic conductance decays and p_f moves up, w will remain in close proximity to w_{p_f}. Throughout the ISI of the free cell the attraction towards p_f will then be sufficient to prevent the trajectory of the quiet cell from jumping up. Next, the trajectory of the quiet cell can only leave the neighbourhood of the stable fixed point p_f, if p_f becomes unstable. This, however, requires that the total synaptic conductance $\bar{g}s$ acting on the quiet cell drops below the release conductance $g^\star$ discussed in section 2.1, that is

$$\bar{g}s < g^\star. \tag{21}$$

The fast time-scale reduction then guarantees that on the slow timescale the trajectory of the quiet cell will jump up instantaneously, becoming free and firing an action potential. As will become evident in the next section, $\dot{w} \gg \dot{s}$ indeed holds for relaxation oscillator type models and fast inhibitory synapses, such as our configuration of the Morris-Lecar model.

In summary: The release condition

$$\bar{g}s = g^\star \tag{22}$$

is sufficient to predict when the quiet cell is released. Due to the symmetry of $n - n$ solutions the release occurs at exactly half the period of the full cycle, that is at $P/2$. The release time therefore uniquely determines the solution. Furthermore, computation of the release time does not depend on the membrane nor the synaptic dynamics of the quiet cell. Instead, the solution of the synaptic variable s of the free cell is sufficient to predict when $\bar{g}s = g^*$ is satisfied. Finally, s is solely determined by the evolution of the depression variable d of the free cell. Constructing a solution $d(t)$ of d during the free phase of either cell will therefore uniquely determine the solution of the full eight-dimensional network. However, finding the solution $d(t)$ requires us to know the initial value $d(0)$ at the start of a cycle at $t = 0$. In the next section we will construct a scalar return map that tracks these initial values $d(0)$ from cycle to cycle of stable $n - n$ solutions.

2.3. Map $\Pi_n : \mathtt{d}_k \mapsto \mathtt{d}_{k+1}$

2.3.1. Rationale

In this section we construct the scalar Poincareé map $\Pi_n : \mathtt{d}_k \mapsto \mathtt{d}_{k+1}$. Here the discrete variable $\mathtt{d}_k$ tracks the values of the continuous depression variable d at the beginning of each $n - n$ burst. The map Π_n therefore describes the change of d, of either of the two cells, from the beginning of one cycle to the beginning of the next cycle. Following the analysis approach taken in Bose and Booth (2011), for now we will assume that the number of spikes in the free phase is known and given by n. Later we will relax this assumption. We will construct Π_n by evolving d first during the free phase and then during the quiet phase of the $n - n$ limit cycle. First, let us give explicit definitions of the free and quiet phases.

Suppose that at $t_1 = 0$ cell 1 becomes free with some initial $d(0)$. Cell 1 then fires n spikes at the uncoupled period T. Let $s(t)$ and $d(t)$ be corresponding solutions of the synapse variables of cell 1. After n spikes the total conductance $\bar{g}s(t)$ acting on the quiet cell 2 has decayed sufficiently to satisfy the release condition (22): that is at some time $t = (n-1)T + \Delta t$ we have $\bar{g}s(t) = g^\star$. Cell 2 is then released and prevents cell 1 from further spiking. Here Δt is the *inter-burst-interval*, or the time between the last spike of cell 1 and the first spike of cell 2 (Bose and Booth, 2011). Once released, cell 2 also fires n spikes until cell 1 becomes free once again at time

$$t = 2(\Delta t + (n-1)T) \equiv P, \tag{23}$$

thus commencing a new cycle. We can now define the free and quiet phases of cell 1 explicitly: The free phase of cell 1 is the time interval between the first and last spikes of the burst, that is for time $0 < t < (n-1)T$. During the free phase of cell 1, the quiet cell 2 is inhibited sufficiently strong to prevent it from firing, hence $\bar{g}s > g^\star$. The quiet phase of cell 1 is the remaining duration of the cycle when cell 2 is bursting, that is when $(n-1)T < t < 2(\Delta t + (n-1)T)$. Note that only the quiet phase depends on Δt. Figure 6 shows a schematic representation of the free and quiet phases.

The quantity Δt will play a central role in the construction of Π_n. From equation (23) it follows that for any given n and $\bar{g}$, Δt is uniquely associated with the period P, and therefore also with the release time of the quiet cell:

$$\Delta t = \frac{1}{2}P - (n-1)T. \tag{24}$$

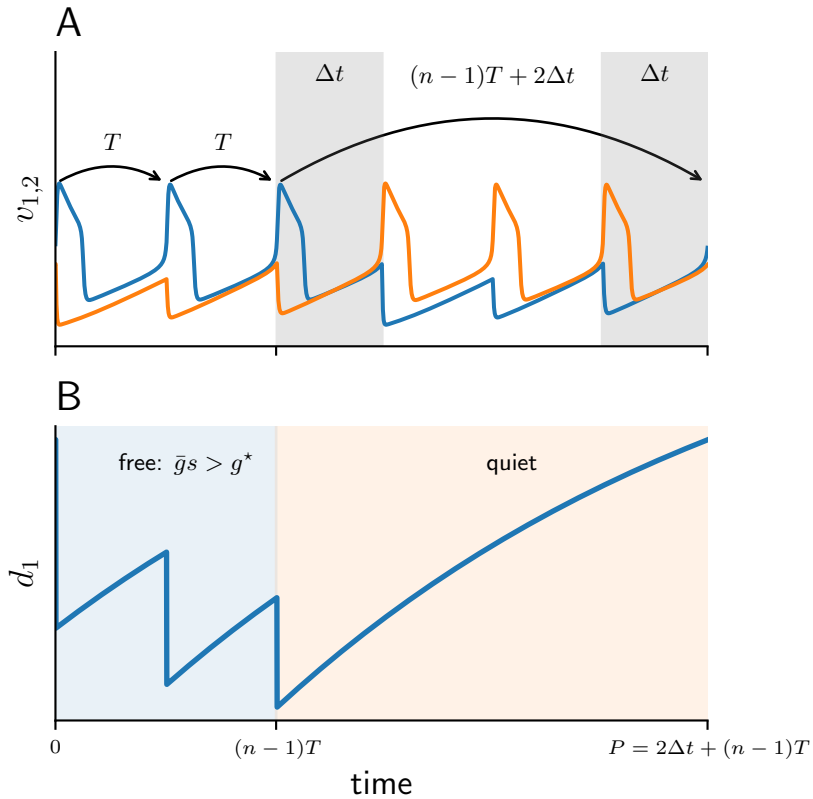

Figure 6: Schematic diagram of the free and quiet phases for a $3-3$ solution. **A**: Membrane potentials of cell 1 (v_1) and cell 2 (v_2). The grey patches depict the two inter-burst-intervals Δt. **B**: Solution $d(t)$ of depression variable of cell 1, during free (blue) and quiet phases (orange).

We can use (24) and the numerically computed bifurcation diagram of P in Figure 5A to obtain the graph of Δt as a function of $\bar{g}$ (Figure 7). $\Delta t(\bar{g})$ is monotonically increasing: stronger coupling $\bar{g}$ increases the total synaptic conductance $\bar{g}s$ that acts on the quiet cell, thus delaying its release. It is easy to see that $\Delta t < T$: once Δt crosses T, the free cell can "squeeze in" an additional spike and the solutions bifurcate into $(n+1)-(n+1)$.

Distinguishing between the free and quiet phases of a cycle allows us to describe the dynamics of the depression variable d explicitly for each phase. As can be seen from Figure 6B, during the free phase d depresses at spike times and recovers in the ISIs. In contrast, during the quiet phase d only

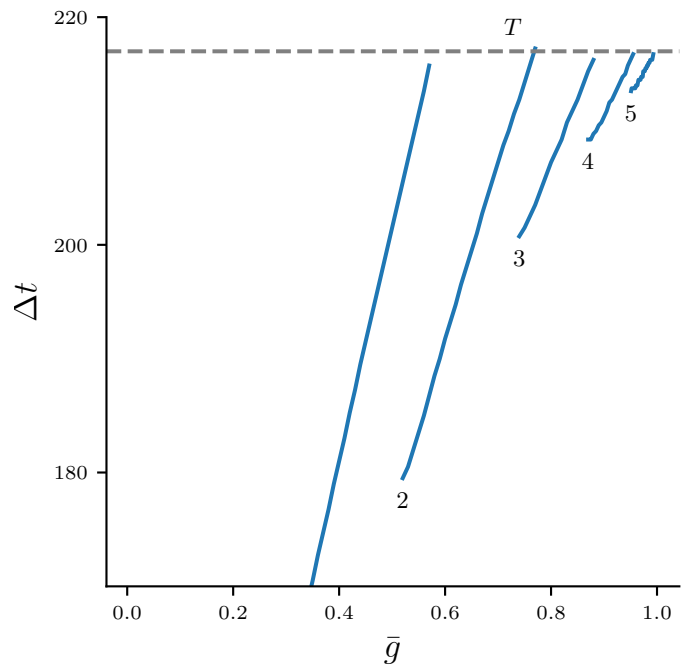

Figure 7: Numerically computed bifurcation diagram of Δt for varying $\bar{g}$. Each continuous branch is associated with a stable $n-n$ burst solution. Increasing $\bar{g}$ increases Δt until the solutions bifurcate at $\Delta t = T$.

recovers and does not depress. Given the initial $\mathtt{d}_k = d(0)$ at the beginning of the cycle and the number of spikes in the free phase n, we can now construct the burst map Π_n. The map $\Pi_n(\mathtt{d}_k) = Q_n(F_n(\mathtt{d}_k))$ is a composition of two maps. Map $F_n : \mathtt{d}_k \mapsto \Delta t$ models the evolution of d in the free phase. F_n takes an initial value $\mathtt{d}_k = d(0)$ and predicts the inter-burst-interval Δt. Map $Q_n : \Delta t \mapsto \mathtt{d}_{k+1}$ models the recovery of d in the quiet phase given some Δt.

2.3.2. Free Phase Map $F_n : \mathtt{d}_k \mapsto \Delta t$

Let us start with map F_n: At each spike time t_k, d depresses with the reset $d(t_k) \leftarrow \lambda d(t_k^-)$ (equation (11)). For the duration of the subsequent ISI ($t_k < t < T + t_k$), the recovery of d is described by the solution to (9):

$$d(t) = 1 - (1 - \lambda d(t_k))e^{-t/\tau_d}. \tag{25}$$

By substituting $t = T$ we can build a linear map $\mathtt{d}_{k+1}$ that models the

depression of d from spike time t_k to the subsequent spike time t_{k+1} during the free phase:

$$\mathtt{d}_{k+1} = \lambda\rho\mathtt{d}_k + (1-\rho), \tag{26}$$

where to keep the notation simple we let $\rho = e^{-T/\tau_d}$ in (26). Since $0 < \lambda, \rho < 1$, the map (26) is increasing and contracting, with a fixed point at

$$d_{sup} = \frac{1-\rho}{1-\lambda\rho}, \tag{27}$$

where $0 < d_{sup} < 1$. As we will see later, d_{sup} is associated with fixed points of the burst map Π_n corresponding to the suppressed solution (see Figure 4E). Solving (26) gives us the linear map $\delta_n : \mathtt{d}_1 \mapsto \mathtt{d}_n$, that for some initial $\mathtt{d}_1 = d(0)$ at $t = 0$ computes $\mathtt{d}_n$ at the nth spike time t_n:

$$\delta_n(\mathtt{d}_1) = \alpha(n)\mathtt{d}_1 + \beta(n), \tag{28}$$

where

$$\alpha(n) = (\lambda\rho)^{n-1}, \tag{29}$$

$$\beta(n) = (1-\rho)\sum_{i=0}^{n-2}(\lambda\rho)^i. \tag{30}$$

Note that $0 < \alpha, \beta < 1$. Figure 8 shows $\delta_n(\mathtt{d}_1)$ for varying n. Since $\lambda < 1$, function δ_n is a linearly increasing function of $\mathtt{d}_1$, decreasing with n. Naturally, δ_n has a fixed point at d_{sup} for all n. Having identified d after n spikes, we can now use the release condition $\bar{g}s = g^\star$ (equation (22)) to find Δt. At the last spike of the free phase at time $t_n = (n-1)T$, synapse variable s is reset according to equation (10):

$$s(t_n) \leftarrow d(t_n^-). \tag{31}$$

Here $d(t_n^-) = \delta_n(d(0))$, and t_n^- is the time just before the nth spike. After the last spike s decays exponentially according to equation (8). Setting the initial value to $d(t_n^-)$ yields:

$$s(t) = d(t_n^-)e^{-\Delta t/\tau_s}, \tag{32}$$

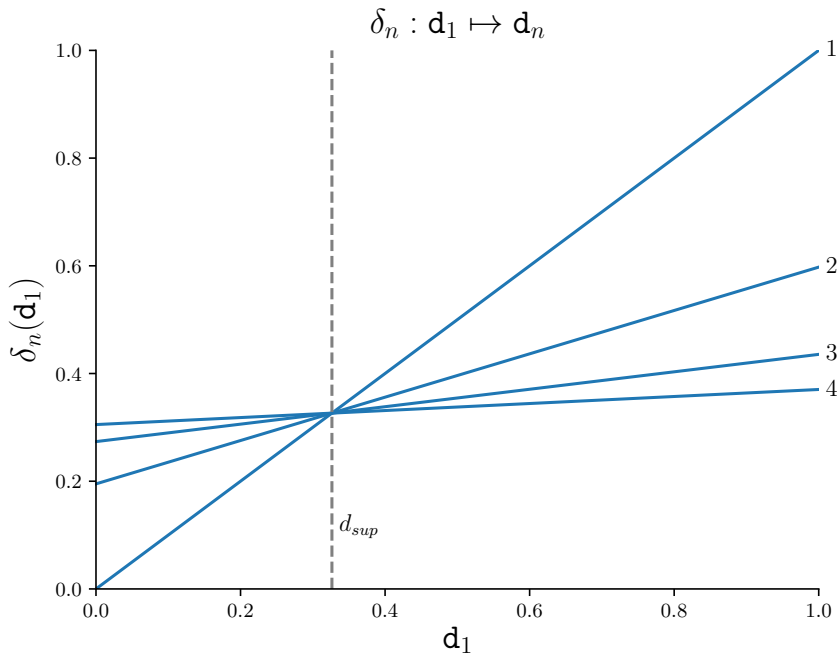

Figure 8: Linear map $\delta_n : \mathtt{d}_1 \mapsto \mathtt{d}_n$ for $n = 1, 2, 3, 4$ with fixed point at d_{sup}.

where $\Delta t < T$. Now, our fast-slow analysis guarantees that the quiet cell 2 will spike and become free when $\bar{g}s - g^\star$ crosses zero. We can therefore formulate the release condition as:

$$\bar{g}d(t_n^-)e^{-\Delta t/\tau_s} = g^\star. \tag{33}$$

Finally, solving for Δt and substituting $\delta_n(\mathtt{d}_k)$ from the equation (28), which relates $\delta_n(d)$ to d and ρ, for $d(t_n^-)$ gives the map F_n:

$$F_n(\mathtt{d}_k) := \tau_s \ln\left(\frac{\bar{g}}{g^\star}\delta_n(\mathtt{d}_k)\right) = \Delta t. \tag{34}$$

Figure 9 shows F_n for varying n.

To elucidate the properties of F_n we will consider negative values of d. However, it is important to note that values $d < 0$ are biologically impossible as d models a finite pool of neurotransmitter, and therefore must be positive. Moreover, the reset of d at spike time in the full system of ODEs according to $d \leftarrow \lambda d$ will always guarantee $d > 0$ since $\lambda > 0$. We will also accept negative

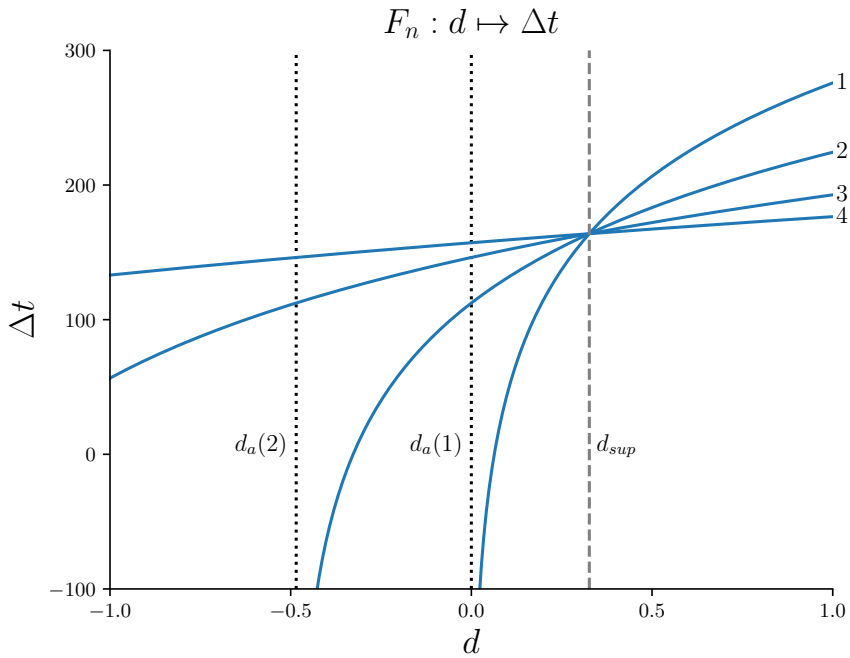

Figure 9: Map $F_n : \mathtt{d}_k \mapsto \Delta t$ for $n = 1, 2, 3, 4$ with corresponding vertical asymptotes at $d_a(n)$ (dotted vertical lines). d_{sup} is indicated by a dashed vertical line.

values of Δt, interpreting them as $n - n$ solutions with partially overlapping bursts. As will become evident, $\Delta t < 0$ is only a formal violation of the biological realism of the map Π_n, as stable $n - n$ solutions of the full system of ODEs system only exist for $\Delta t > 0$.

It is easy to show that F_n is a strict monotonically increasing function of $\mathtt{d}_k$. Larger values of $\mathtt{d}_k$ at burst start cause stronger inhibition of the quiet cell, and therefore prolong its release time and the associated Δt. Map F_n is defined on $(d_a, 1)$, where d_a is a vertical asymptote for $\delta_n = 0$ with

$$d_a(n) = -\frac{\beta(n)}{\alpha(n)} < 0. \tag{35}$$

The curves F_n for all $n > 0$ intersect at d_{sup}. We can now use the release condition (22) to find the corresponding coupling strength $\bar{g}_{sup}$ that will produce full suppression solutions. We write $\bar{g}_{sup}$ as a function of the depression strength λ:

$$\bar{g}_{sup}(\lambda) = \frac{g^\star e^{T/\tau_s}}{d_{sup}}. \tag{36}$$

$$\tag{37}$$

Substituting (27) for d_{sup} yields:

$$\bar{g}_{sup}(\lambda) = g^\star e^{T/\tau_s} \frac{1-\lambda\rho}{1-\rho}. \tag{38}$$

Note that the above dependence of $\bar{g}_{sup}$ on λ is linear and monotonically decreasing. A biological interpretation of the monotonically decreasing $\bar{g}_{sup}(\lambda)$ is easy to find: Increasing λ reduces the strength of the depression of the free cell. This in turn allows the free cell to fully suppress the quiet cell at smaller values of $\bar{g}$.

2.3.3. Quiet Phase Map $Q_n : \Delta t \mapsto \mathtt{d}_{k+1}$

We now turn to the construction of map $Q_n : \Delta t \mapsto \mathtt{d}_{k+1}$. Q_n describes the recovery of d during the quiet phase. As we have identified earlier, the recovery in the quiet phase lasts for $2\Delta t + (n-1)T$. Substituting that into the recovery equation (25) yields the map Q_n:

$$Q_n(\Delta t) := 1 - (1 - \lambda \mathtt{d}_n) e^{-(2\Delta t + (n-1)T)/\tau_d}. \tag{39}$$

Here $\mathtt{d}_n$ is the value of the depression variable at the last spike t_n of the free phase. Given Δt, we solve the release condition (22) for $\mathtt{d}_n$:

$$\mathtt{d}_n = \frac{g^\star}{\bar{g}} e^{\Delta t/\tau_s}. \tag{40}$$

Map Q_n is shown in Figure 10 for various values n. $Q_n(\Delta t)$ is monotonically increasing as larger values Δt imply a longer recovery time, and hence Q_n grows without bound. All curves Q_n intersect at some $\Delta t = \tau_s \ln \frac{\bar{g}}{g^\star \lambda}$ where

$$Q_n\left(\tau_s \ln \frac{\bar{g}}{g^\star \lambda}\right) = 1. \tag{41}$$

As we will show in the next section, all fixed points of the full map Π_n occur for $\mathtt{d}_k < 1$. We will therefore restrict the domain of Q_n to $(-\infty, \ln(\frac{\bar{g}}{g^\star \lambda})\tau_s)$ and the codomain to $(-\infty, 1)$.

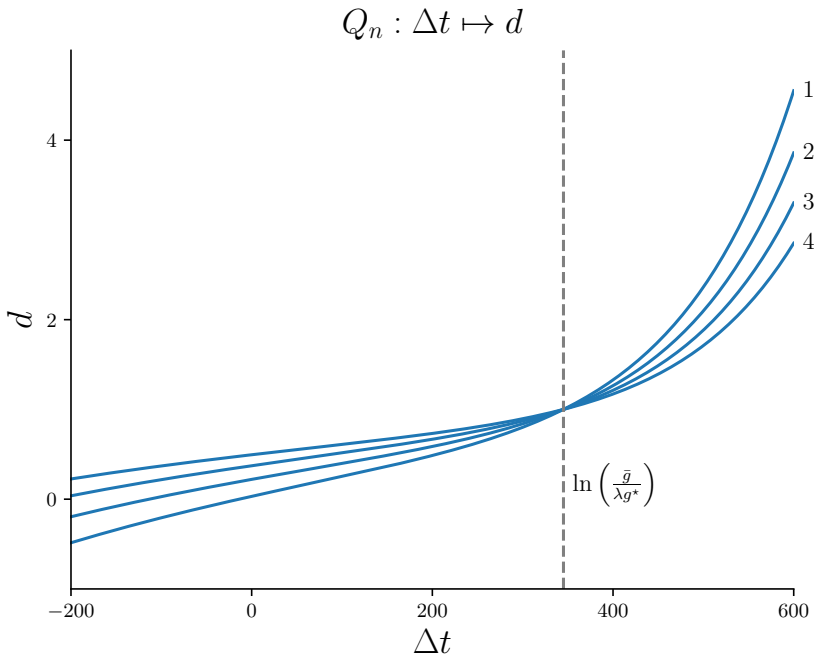

Figure 10: Quiet phase map $Q_n : \Delta t \mapsto \mathtt{d}_{k+1}$ for $n = 1, 2, 3, 4$. Intersection of curves Q_n for all n occurs at $\Delta t = \ln \frac{\bar{g}}{\lambda g^\star}$ (dashed line).

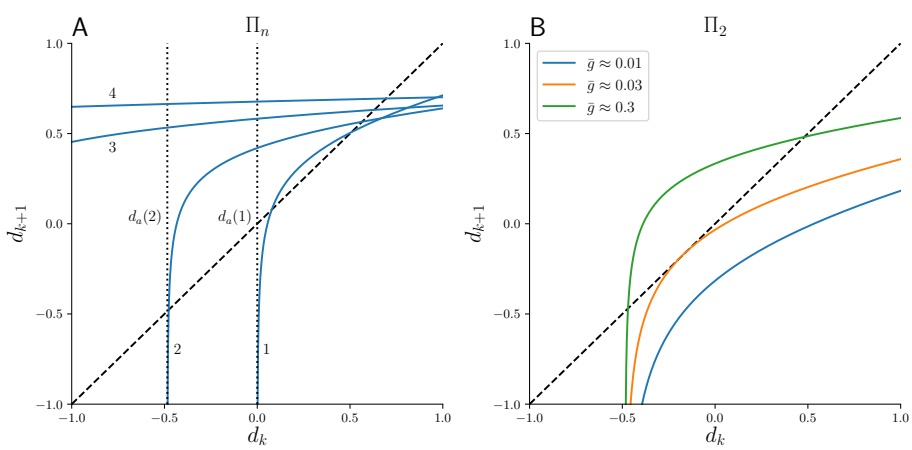

Figure 11: Map $\Pi_n : \mathtt{d}_k \mapsto \mathtt{d}_{k+1}$. **A**: Π_n for $n = 1, 2, 3, 4$ at $\bar{g} = 0.6$. **B**: Π_2 with $n = 2$ for varying $\bar{g} \approx 0.01, 0.034, 0.3$. Identity function is illustrated by a diagonal line.

2.3.4. Composition Map $\Pi_n : \mathtt{d}_k \mapsto \mathtt{d}_{k+1}$

Having found F_n and Q_n, we can now construct the full map $\Pi_n(\mathtt{d}_k) = Q_n[F_n(\mathtt{d}_k)]$:

$$\Pi_n(\mathtt{d}_k) := 1 - \frac{\rho^{n-1} g^{\star\tau} \delta_n^{-\tau}(\mathtt{d}_k)(1 - \lambda\delta_n(\mathtt{d}_k))}{\bar{g}^\tau}, \tag{42}$$

where we substituted $\tau = 2\tau_s/\tau_d$. Since d is the slowest variable and $\tau_d > \tau_s$, we assume $\tau < 1$. Figure 11A depicts Π_n for various n. Just as F_n, map Π_n is defined on $(d_a(n), 1)$. Intersections of Π_n with the diagonal at some $d^\star$ with $\Pi_n(d^\star) = d^\star$ are fixed points of the map. Varying the synaptic strength $\bar{g}$ moves the curves Π_n up and down the (d_k, Π_n)-plane. Figure 11B shows Π_2 with $n = 2$. For $\bar{g} < 0.03$ Π_2 has no fixed points. As $\bar{g}$ is increased to $\bar{g} \approx 0.03$, Π_2 coalesces with the diagonal tangentially. When $\bar{g} > 0.03$, a pair of fixed points emerge, a stable $d^\star_-$ and an unstable $d^\star_+$, indicating the occurrence of a fold bifurcation of maps.

Finding fixed points $d^\star$ explicitly for all $n > 0$ is not trivial. However, we can use equation (11) to determine $d^\star$ implicitly. Let Φ_n describe the fixed points of Π_n:

$$\Phi_n(d^\star) := \Pi_n(d^\star) - d^\star = 0. \tag{43}$$

Then the derivative with respect to $\bar{g}$ is calculated as

$$D_{\bar{g}}\Phi_n(d^\star) = \tau \frac{\rho^{n-1} g^{\star\tau} \delta_n^{-\tau}(d^\star)(1 - \lambda\delta_n(d^\star))}{\bar{g}^{\tau+1}}. \tag{44}$$

We can see that the sign of $D_{\bar{g}}\Phi_n$ is determined by the sign of $1 - \lambda\delta_n(d^\star)$. Solving $1 - \lambda\delta_n(d^\star) = 0$ for $d^\star$ by applying the definition of δ_n in equation (28) yields

$$d^\star = \frac{\lambda^{-1} - \beta(n)}{\alpha(n)} =: d_\phi(n). \tag{45}$$

Simple calculations reveal that $d_\phi(n)$ is strictly increasing with n:

$$d_\phi(n+1) - d_\phi(n) = \frac{\lambda^{-1} - 1}{(\lambda\rho)^n} > 0 \text{ for all } n > 0. \tag{46}$$

Since $d_\phi(n = 1) = \lambda^{-1} > 1$ for $\lambda \in (0, 1)$, we can conclude that $D_{\bar{g}}\Phi_n > 0$ for all $d^\star < 1$ and all $n > 0$. This allows us to utilise the implicit function theorem to express $\bar{g}$ as a function of $d^\star$, and solving equation (43) for $\bar{g}$ we

then get the synaptic coupling strength $\bar{g}(d^\star)$ that corresponds to the fixed point $d^\star$:

$$\bar{g}(d^\star) = g^\star \left(\frac{\rho^{n-1}\delta_n^{-\tau}(d^\star)(1-\lambda\delta_n(d^\star))}{1-d^\star} \right)^{1/\tau}. \tag{47}$$

The graph of the inverse of $\bar{g}(d^\star)$ is shown in Figure 12 (blue line). Note the typical quadratic shape of a fold bifurcation. It is also evident from Figure 11B that for $\lambda = 0.5$ the fold bifurcations occur for increasingly smaller $\bar{g}$ as n is increased. In the remaining part of this section we will show that all fixed points $d^\star$ for all $n > 1$ are indeed created via fold bifurcations of maps. To show that our derivation of $\bar{g}(d^\star)$ works we also compute the curves numerically using the conventional Newton-Raphson method (Press, 2007) (orange dots). As we will show below, map $\Pi_n(\mathtt{d}_k)$ is monotonically increasing, and the root-finder is therefore guaranteed to converge (with at least quadratic rate) to the two roots (if any exist) if initialised at $d_a(n)$ and 1.

2.3.5. Fold Bifurcations of Π_n

The derivative of $\Pi_n(\mathtt{d}_k)$ is given by

$$D\Pi_n(\mathtt{d}_k) = \frac{\tau_s \alpha \rho^{n-1} g^{\star\tau} \left(\frac{2}{\tau_{\mathtt{d}_k}} \delta_n^{-(\tau+1)}(\mathtt{d}_k) + \frac{\tau_d - 2\tau_s}{\tau_d \tau_s} \lambda \delta_n^{-\tau}(\mathtt{d}_k) \right).}{\bar{g}^\tau} \tag{48}$$

It is straightforward to show that Π_n is strictly monotonous with $D\Pi_n > 0$ and $D^2\Pi_n < 0$. In the limit $\mathtt{d}_k \to d_a$ the slope $D\Pi_n$ is unbounded, and since $D^2\Pi_n < 0$ there exists a unique $d^\star$ for any $\bar{g} > 0$ such that $D\Pi_n(d^\star) = 1$. For $\mathtt{d}_k < 1$, it is also evident that $D_{\bar{g}}\Pi_n > 0$. Since $\lim_{\bar{g}\to 0} \Pi_n$ is unbounded and $\lim_{\bar{g}\to\infty} \Pi_n = 1$ for $d > d_a$ and any $n > 0$, it follows then by the intermediate value theorem that there exists some $\bar{g}_c > 0$ and $d_c \in (d_a, 1)$ such that $\Pi_n(d_c)|_{\bar{g}=\bar{g}_c} = d_c$, and $D\Pi_n(d_c) = 1$. That is, every curve Π_n undergoes a fold bifurcation by intersecting the diagonal tangentially at some d_c and creating two fixed points, one stable and one unstable. Here $D^2\Pi_n(\mathtt{d}_k) < 0$ and $D_{\bar{g}}\Pi_n > 0$ constitute the nondegeneracy conditions (e.g. see Kuznetsov, 2004) indicating that in a neighbourhood of $(d_c, \bar{g}_c)$, map $\Pi_n(\mathtt{d}_k)$ has the topological normal form of a codimension-1 fold bifurcation, that is $y \mapsto \beta + y - y^2$, where $y \in \mathbb{R}$ and $\beta \in \mathbb{R}$.

The above conclusion not only signifies that all fixed points of Π_n are created via fold bifurcations of maps, but most importantly, that for n and $\bar{g}$

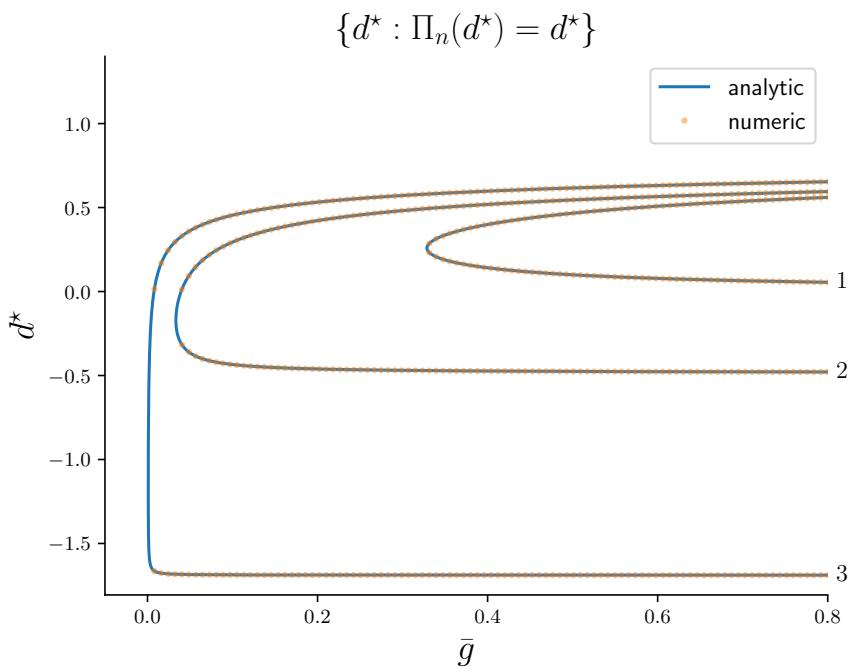

Figure 12: Analytically (blue line) and numerically (orange dots) computed fixed points $d^\star$ of map Π_n for varying $\bar{g}$ and $n = 1, 2, 3$.

large enough, maps Π_n have a stable fixed point. In fact, we can show that for any finite coupling strength $\bar{g} > 0$, there exists some $N > 0$, such that for all $n > N$ the map Π_n has a stable fixed point. Consider the point $\mathtt{d}_k = d_{sup}$ (equation (27)), where $\delta_n(d_{sup}) = d_{sup}$ for any $n > 0$. Then from equations (42) and (48) it follows that

$$\Pi_n(d_{sup}) < \Pi_{n+1}(d_{sup}). \tag{49}$$

In the limit $n \to \infty$ we have

$$\lim_{n\to\infty} \Pi_n(d_{sup}) = 1 > d_{sup}. \tag{50}$$

Since $\Pi_n(d_{sup})$ is monotonically increasing with n, it follows that for any $\bar{g} > 0$ there exists some $N > 0$ such that $\Pi_N(d_{sup}) > d_{sup}$. The monotonicity of Π and $D\Pi$ with respect to $\mathtt{d}_k$ then implies that Π_N has a pair of fixed points on $(d_a, 1)$. We can see long-cyclic bursts in the full system of ODEs in Figure 13. Note that while the map predicts stable $n - n$ solutions for

any $\bar{g} < \bar{g}_{sup}$ sufficiently large, these solutions occur on increasingly small parameter intervals of $\bar{g}$, which makes identifying them in the ODE system numerically challenging.

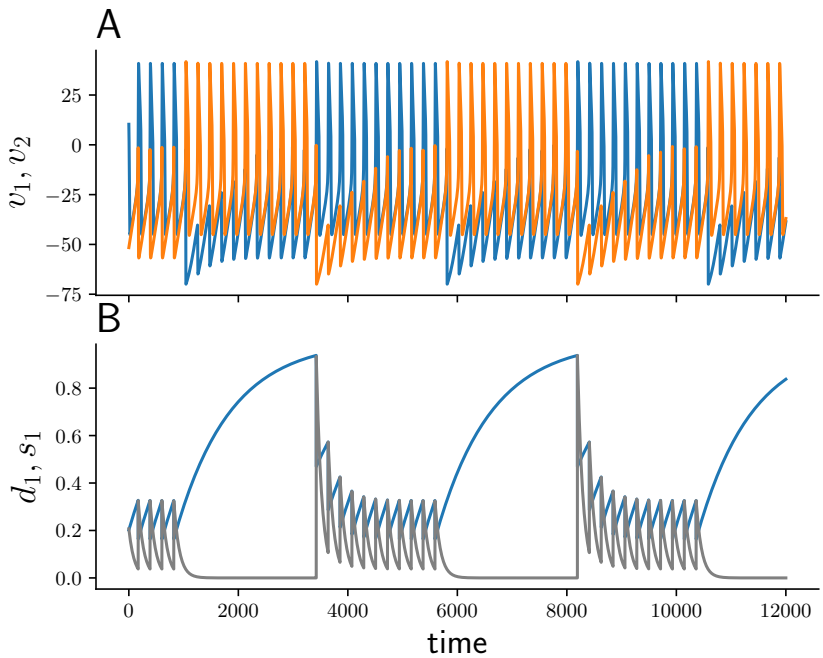

Figure 13: Long-cyclic $11-11$ burst solution with $\bar{g} = 1.015$. **A**: Membrane potentials v_1 and v_2 of the two cells. **B**: Synaptic variables d_1 and s_1 of first cell.

Deriving the exact parameters $(\bar{g}, \lambda)$ for each n associated with the fold bifurcations is not straightforward. However, in the limit $\lambda \to 1$ the equations (48) and (42) become more manageable. To provide a better intuition for the map we will therefore demonstrate the fold bifurcations in the theoretical case of total absence of depression, that is when $\lambda = 1$. This scenario can be associated with a full suppressed solution. In this case $\Pi_n|_{\lambda=1}$ simply models the exponential recovery of d according to equation (9) for $0 < t < 2(\Delta t + (n-1)T) = P$:

$$\Pi_n(\mathtt{d}_k)|_{\lambda=1} = 1 - (1 - \mathtt{d}_k)e^{-2\Delta t/\tau_d}\rho^{2(n-1)}. \tag{51}$$

Equation (51) has a fixed point at $d^\star = 1$ for all $n > 0$, which allows us to find $\Delta t = F_n(1)$. We obtain:

$$\Pi_n(\mathtt{d}_k = 1)|_{\lambda=1} = 1 - (1 - \mathtt{d}_k)\left(\frac{\bar{g}}{g^\star}\right)^{-\tau} \rho^{2(n-1)}. \tag{52}$$

Parameter values $\bar{g}$ that are associated with the fold bifurcations satisfy equation $D\Pi_n(d = 1)|_{\lambda=1} = 1$, solving for $\bar{g}$ gives

$$\bar{g}_f(n) = g^\star \rho^{2(n-1)/\tau} = g^\star \exp\left(\frac{-(n-1)T}{\tau_s}\right), \tag{53}$$

where $\bar{g}_f(n)$ denotes the fold bifurcation value of $\bar{g}$ as a function of n. Figure 14 depicts the values of $\bar{g}_f(n)$ for increasing n in the limit $\lambda \to 1$ (orange), as well when $\bar{g}_f(n)$ is numerically computed for $\lambda = 0.5$ (blue) using a conventional Simplex minimisation (Nelder and Mead, 1965) of $\bar{g}(d^\star)$ (equation (47)).

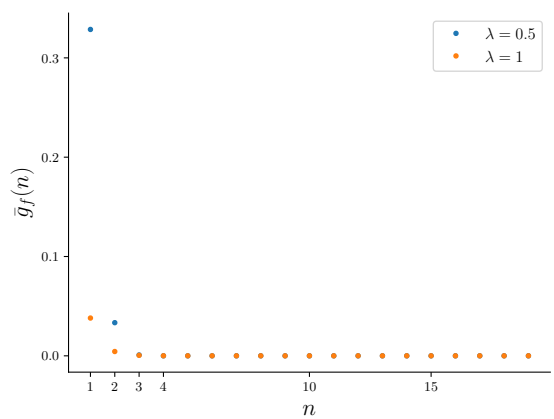

Figure 14: Values of $\bar{g}$ associated with fold bifurcations computed numerically for $\lambda = 0.5$ (blue) and found explicitely in the limit $\lambda \to 1$ (orange) for increasing n.

2.4. Map $\Pi : \mathtt{d}_k \mapsto \mathtt{d}_{k+1}$

2.4.1. Rationale

Having now gained an understanding of how different $n - n$ solutions are created and what determines the shape of the bifurcation diagram, let us remove the assumption that the free phase of a cycle contains exactly n spikes. The main effect of removing this assumption is that now n has to be found explicitly for any $\mathtt{d}_k = d(0)$ at the cycle start. We will find

n recursively by iterating through the spike times of the free cell until the release condition (22) predicts the firing of the previously quiet cell. This will yield the recursive map $F : \mathtt{d}_k \mapsto L$, that now returns the burst length L given some initial $\mathtt{d}_k = d(0)$. Given L, variable d can be easily evolved during the quiet phase with the map $Q : L \mapsto \mathtt{d}_{k+1}$. In analogy to the previous section, we define the composite burst map as $\Pi(\mathtt{d}_k) = Q[F(\mathtt{d}_k)]$ (without subscripts).

2.4.2. Free Phase Map $F : \mathtt{d}_k \mapsto L$

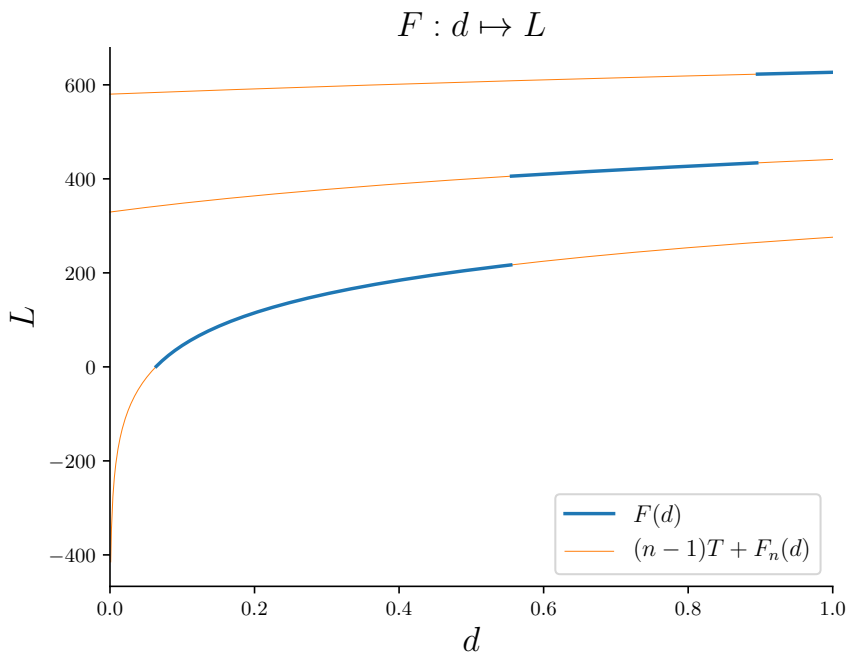

Figure 15: Recursive map $F : \mathtt{d}_k \mapsto L$ (blue) in comparison to the map $F_n : \mathtt{d}_k \mapsto \Delta t$ (orange) for $n = 1, 2, 3$. The output of $F_n(\mathtt{d}_k)$ has been transformed to $(n-1)T + F_n(\mathtt{d}_k)$ in order to match $F(\mathtt{d}_k)$.

Let us start with the map $F : \mathtt{d}_k \mapsto L$ that models the depression of d during the free phase. At each spike time, we will test whether the total synaptic conductance is sufficient to allow cell 1 to fire another spike, or whether cell 2 becomes free and terminates the burst of cell 1. As in the previous section, let us assume that cell 1 becomes free and produces an action potential at $t = 0$ with some initial $\mathtt{d}_k = d(0)$ and, naturally, a

$L(0) = 0$. This means that the total synaptic conductance acting on the quiet cell 2 is given by $\bar{g}\mathtt{d}_k e^{-t/\tau_s}$ (equation (32)). The release condition (22) determines whether cell 2 becomes free after some $t = \Delta t$, or whether cell 1 fires at least another spike at $t = T$. If there exists a $t < T$ such that

$$\bar{g}\mathtt{d}_k e^{-t/\tau_s} < g^\star. \tag{54}$$

then cell 2 becomes free before cell 1 can fire another spike. The exact time Δt can be found by solving the release condition (22) for Δt with the substitution $s = \mathtt{d}_k e^{-\Delta t/\tau_s}$:

$$\Delta t = \tau_s \ln\left(\frac{\bar{g}}{g^\star}\mathtt{d}_k\right). \tag{55}$$

In contrast, if the inhibitory conductance is sufficient to keep cell 2 quiet for at least $t = T$, then

$$\bar{g}\mathtt{d}_k e^{-T/\tau_s} > g^\star \tag{56}$$

holds, and cell 1 can produce one more spike. In this case, L will be at least of length T and we set:

$$L = L(0) + T. \tag{57}$$

We can find the value of the depression variable at the next spike of cell 1 at time $t = T$ by evolving d according to equation (25):

$$d(T^-) = 1 - (1 - \lambda\mathtt{d}_k)\, e^{-T/\tau_d}. \tag{58}$$

Now we are in a position to repeat the preceding procedure and test once more whether the quiet cell will remain quiet for a duration T. Assume that after n spikes d will be sufficiently depressed to release the quiet cell before the subsequent spike of the free cell. The exact time of that release will be then given by the previously accumulated burst duration L and the inter-burst-interval Δt. For a free phase consisting of n spikes the release time L of the quiet cell is given by

$$L = (n-1)T + \tau_s \ln\left(\frac{\bar{g}}{g^\star}\mathtt{d}_n\right). \tag{59}$$

This iterative procedure allows us to define F recursively. Given some initial $F_0 = L(0) = 0$, we define

$$F(\mathtt{d}_k) := \begin{cases} T + F\left(1 - (1 - \lambda \mathtt{d}_k)e^{-T/\tau_d}\right) & \text{if } \bar{g}\mathtt{d}_k e^{-T/\tau_s} > g^\star, \\ \tau_s \ln \frac{\bar{g}\mathtt{d}_k}{g^\star} & \text{otherwise.} \end{cases} \tag{60}$$

Note that as we update the input of the recursive call to F with

$$\mathtt{d}_{k+1} \leftarrow 1 - (1 - \lambda \mathtt{d}_k)e^{-T/\tau_d}, \tag{61}$$

we also implicitly track the evolution of d. Figure 15 shows the partially continuous map F, and the previously constructed continuous map F_n for various n. Since F_n returns Δt and not L, we have added $(n-1)T$ to each curve of F_n to have matching axes. This way it becomes evident that each continuous interval of F corresponds to a release time L consisting of n spikes, and therefore overlaps with the respective curve F_n.

2.4.3. Quiet Phase Map $Q : L \mapsto \mathtt{d}_{k+1}$

Given the release time of the quiet cell L, determining the recovery from depression of cell 1 via the map $Q : L \mapsto \mathtt{d}_{k+1}$ is straightforward. The duration of the quiet phase is given by $(n-1)T + 2\Delta t = L + \Delta t$. We can find Δt directly from the definition of L in (59):

$$L = (n-1)T + \Delta t. \tag{62}$$

Since n is unknown, we can use the remainder to find Δt:

$$\Delta t = L \bmod T \text{ for } L > 0. \tag{63}$$

Then map Q is defined by:

$$Q(L) = 1 - (1 - \lambda \mathtt{d}_n)e^{-(L+\Delta t)/\tau_d}. \tag{64}$$

Here $\mathtt{d}_n$ is the value of the depression variable at the last spike of the free phase. We can find $\mathtt{d}_n$ as in equation (40), that is

$$\mathtt{d}_n = \frac{g^\star}{\bar{g}} e^{\Delta t/\tau_s}. \tag{65}$$

Figure 16 shows the partially continuous map $Q : L \mapsto \mathtt{d}_{k+1}$ and the continuous map $Q_n : \Delta t \mapsto \mathtt{d}_{k+1}$ for $n = 1, 2, 3, 4, 5$. To match the axes of both maps Q and Q_n, we have transformed the domain of Q_n according to

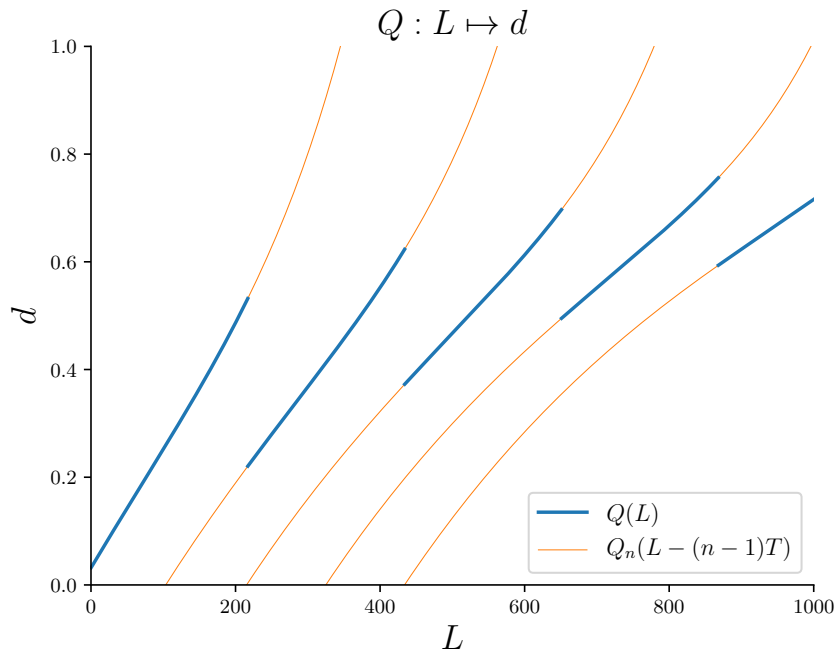

Figure 16: Partially continuous map $Q : L \mapsto \mathtt{d}_{k+1}$ (blue) in comparison to the continuous map $Q_n : \Delta t \mapsto \mathtt{d}_{k+1}$ (orange) for $n = 1, 2, 3, 4, 5$. To match the axis of both maps, the domain of Q_n has been transformed according to $\Delta t = L - (n-1)T$.

$\Delta t = L-(n-1)T$. Just as with F, each continuous interval of Q corresponds to a recovery duration consisting of n spikes, and therefore overlaps with the associated curve Q_n.

2.4.4. Composition Map $\Pi : \mathtt{d}_k \mapsto \mathtt{d}_{k+1}$

We can compute the full map $\Pi : \mathtt{d}_k \mapsto \mathtt{d}_{k+1}$ numerically, by first calculating the burst length $L = F(\mathtt{d}_k)$, and then finding the return value $\mathtt{d}_{k+1} = Q(L)$:

$$\Pi(\mathtt{d}_k) = Q[F(\mathtt{d}_k)]. \tag{66}$$

Figure 17A shows map Π and the curves Π_n for $\bar{g} = 0.65$ and $n = 1, 2, 3$, and Figure 17B depicts Π for increasing values of $\bar{g}$. Π is a partially continuous map, where each continuous interval associated with some n is described by a curve Π_n. Therefore, all qualitative descriptions of Π_n regarding monotony, slope, and dependence on $\bar{g}$ also hold for Π on the respective continuous

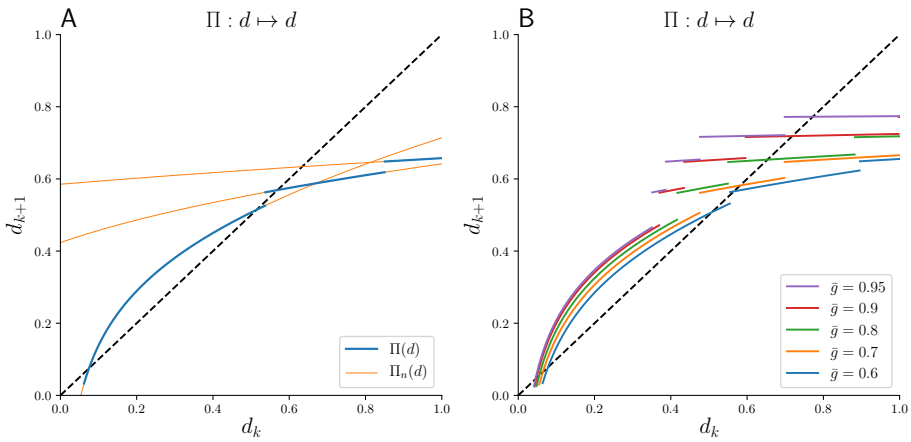

Figure 17: **A**: Partially continuous and recursive map Π (blue) in comparison to the continuous map Π_n (orange) for $n = 1, 2, 3$ and $\bar{g} = 0.62$. Π is bistable with two stable fixed points. **B**: Map Π for increasing parameter values $\bar{g}$.

intervals. Most importantly, it follows that for $\bar{g}$ sufficiently large, Π has at least two fixed points, one of which is stable. Stable fixed points $d^\star$ of Π are associated with stable $n - n$ solutions of the flow system, and can be interpreted as the maximum values of d at the start of the cycle (see Figure 18B).

We have previously shown that for any finite range of coupling strengths with $\bar{g} < g_{sup}$, there exists an infinite number of maps Π_n with some corresponding number n that have a stable fixed point. This also means that Π has stable fixed points linked to stable $n - n$ solutions for any n sufficiently large. In other words, given that our reduction assumptions hold, a two-cell reciprocally inhibitory network with depression can produce an infinite number of anti-phase burst patterns (of increasing period) for a finite coupling strength interval.

We also observe that there exist some values of $\bar{g}$, such as $\bar{g} = 0.76$ in Figure 17A, where Π has two stable fixed points. Figure 18A shows a numerically computed cobweb plot of Π for $\bar{g} = 0.76$ with initial values at 0.1 (blue lines) and 1.0 (orange lines) respectively. Both sequences approach the respective stable fixed points (blue and orange dots) after a number of iterations of Π. Figure 18B depicts the associated $2 - 2$ (bottom, blue) and $3 - 3$ (top, orange) solutions of the depression variable from numerical simulations of full ODE system. Bose and Booth (2011) have previously

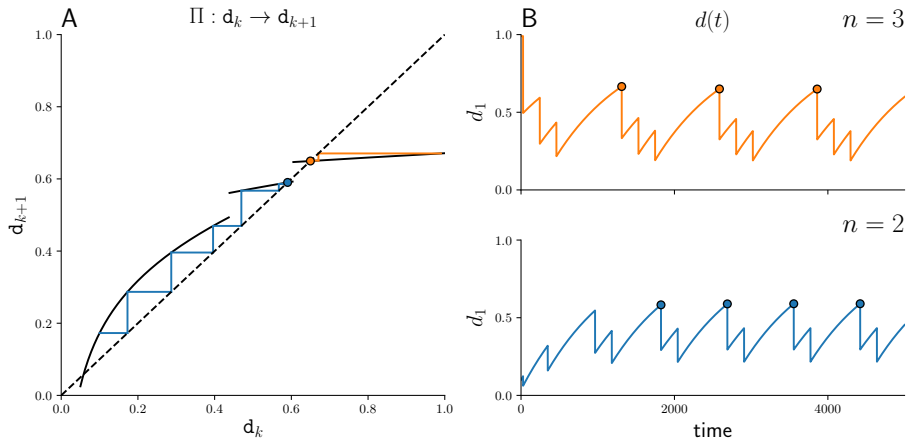

Figure 18: **A**: Cobweb diagram of $\Pi : \mathtt{d}_k \mapsto \mathtt{d}_{k+1}$ for $\bar{g} = 0.76$. Numerical iterations are initialised at $\mathtt{d}_1 = 0.1$ and $\mathtt{d}_1 = 1.0$ and quickly converge to the two stable fixed points (blue and orange dots) respectively. **B**: Corresponding solution profiles acquired from numerically integrating the system of ODEs. Orange and blue dots represent values $\mathtt{d}_k$ in close neighbourhood to the fixed points of Π, corresponding to $3-3$ (top) and $2-2$ (bottom) bursts respectively.

shown the existence of bistability in a very similar network for $n < 3$.

We compute these fixed points numerically to derive the full bifurcation diagram. Figure 19 illustrates two bifurcation diagrams: One diagram that has been used in Figure 5 (blue lines) and computed by simulating the original system of ODEs. The other diagram has been found by numerically identifying stable fixed points of Π (orange). Note that our reduction approach relies on the assumption that the total synaptic conductance $\bar{g}s$ is sufficiently large. This may explain the better match between the two diagrams for larger values of $\bar{g}$. However, even for large $n - n$ burst solutions there is a mismatch between the curves, in particular at the left and right boundaries close to the period increments. Presumably the assumptions on the time scales of w and s dynamics do not hold here and can only be captured by more complex approximations.

2.5. Conclusion

To study the mechanisms of burst generation in tadpole struggling we have analysed a neuronal network that consists of a pair of inhibitory neurons that undergo a frequency dependent synaptic depression. We have shown

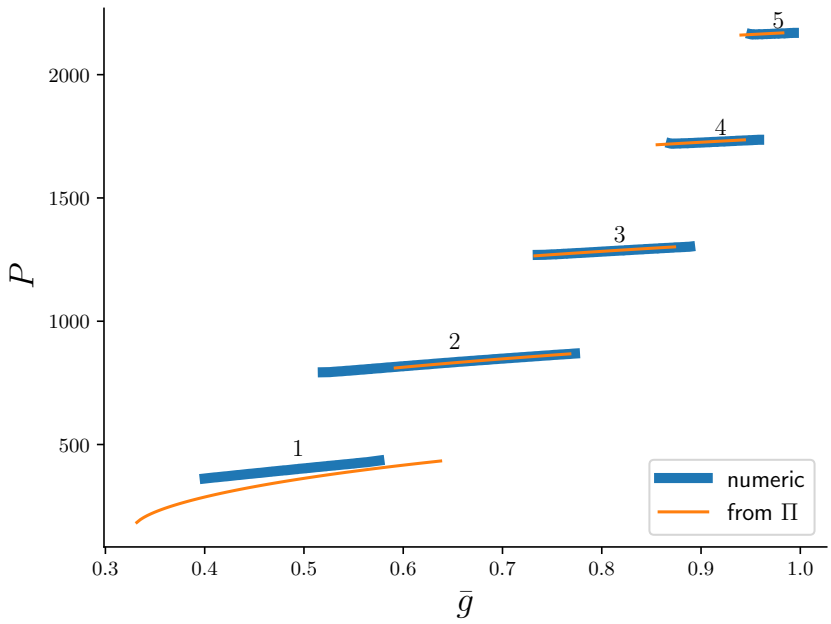

Figure 19: Numerically computed bifurcation diagram (blue) of period P as a function of $\bar{g}$, in comparison to curves found from stable fixed points of map Π (orange).

that when the strength of inhibition between the neurons is varied, such a simple network can display a range of different struggling-like $n-n$ burst patterns. We have applied methods of geometric singular perturbation theory to reduce network model of eight ODEs to a scalar first return map Π of the slow depression variable d. This map Π is a composition of two maps, F and Q, that model the evolution of d during the free and quiet phases of $n-n$ solutions respectively. Both F and Q maps are constructed by using the dynamics of single uncoupled neurons. We have then proved the existence and stability of fixed points of Π, which are created in pairs through a fold bifurcation of maps, where the stable fixed point correspond to stable $n-n$ burst solutions of the full two-cell system of ODEs. The results from our one dimensional map match excellently with numerical simulation of the full struggling network.

We have studied anti-phase $n-n$ solutions, assuming that the synaptic coupling $\bar{g}$ between the two cells is symmetrical. However, Bose and Booth

(2011) have shown that asymmetrical coupling can result in network solutions of type $m{-}n$, where one cell fires m spikes, while the other n. It is conceivable that our map construction can be extended to also describe $m-n$ solutions. Remember, in the case of symmetrical coupling and assuming $n{-}n$ solutions, we had to build one map F_n for the free phase, and another map Q_n for the quiet phase. With asymmetrical coupling, one would have to account for solutions of both the $m{-}n$ and $n{-}m$ types. To do that, one could construct a two-dimensional map that tracks the depression variables d_1 and d_2 of both cells. Generally speaking, our map construction approach is applicable to any small network, even with more than two neurons. The main obstacle lies in identifying all combinations of different solutions. Another drawback of our reduction approach is the strictness of assumptions about the time-scale disparity in the system. That is, the method is only applicable to neuronal models with membrane dynamics that are not too slow, e.g. such as the slow calcium-dependent T-current analysed in Matveev et al. (2007). A network with synaptic depression and neurons with slow membrane currents would possibly involve dynamics that occur on at least three timescales. In theory, however, the methods of singular perturbation can also be applied to systems with more than two timescales (e.g. Kuehn, 2015).

We have shown that synaptic depression of inhibition allows a half-centre network to produce an infinite number of stable burst solutions of arbitrarily long period, on a finite interval of synaptic strengths. While we have identified the bifurcations of the reduced map, we have not found the corresponding bifurcations of the flow system. However, our results are reminiscent of a saddle homoclinic orbit bifurcation, where a stable periodic orbit collides with a saddle equilibrium, and its period becomes infinite. A number of theoretical studies have investigated such a *homoclinic tangency to a periodic orbit* in higher-dimensional systems (e.g. Gavrilov and Shilnikov, 1972; Gaspard and Wang, 1987), and a next step would be to provide a rigorous explanation of not only the map dynamics, but also of the flow dynamics.

2.6. Acknowledgements

Funding for this study was provided by the Wellcome Trust Doctoral Training Programme in Neural Dynamics, Grant no. 099699/Z/12/Z.

We thank Prof Alan Chmapneys for sharing his insights on non-continuous maps during the course of this research. We are also grateful to Prof Alan Roberts and Dr Stephen R. Soffe for their comments on earlier versions of the manuscript.

2.7. Appendix: Computing bifurcation diagram numerically

The bifurcation diagram of stable $n-n$ solutions of the two-cell network in Figure 5 is obtained numerically as follows: We initialise the coupling strength at parameter values associated with one type of $n-n$ solution, that is we choose the values $\bar{g} = 0.4, 0.7, 0.8, 0.9, 0.98$ for the $1-1$, $2-2$, $3-3$, $4-4$, and $5-5$ solutions respectively. For each $\bar{g}$ the system is then numerically integrated sufficiently long for any transients to fully subside. We then identify one period of the solution by finding the first return of the depression variable d_1. That is, we choose some value $\mathtt{d}_k$ at a spike time t_k, and by iterating from spike to spike find some subsequent value $\mathtt{d}_{k+1}$ at spike time such that $|\mathtt{d}_{k+1} - \mathtt{d}_k| < \epsilon$. If a periodic solution of type $n-n$ is found in such way, $\bar{g}$ is step-wise increased/decreased, and the above algorithm is repeated. Otherwise, the set of all previously found solutions and the corresponding values $\bar{g}$ are returned.

Note that applying conventional methods of numerical continuation is not straightforward for our model, as the discontinuous resets in equations (10) and (11) make the root finding challenging (e.g. see Kuznetsov, 2004, for continuation methods).

3. References

Bose, A. and Booth, V. (2011). Co-existent activity patterns in inhibitory neuronal networks with short-term synaptic depression. *Journal of Theoretical Biology*, 272(1):42–54.

Bose, A., Manor, Y., and Nadim, F. (2001). Bistable oscillations arising from synaptic depression. *SIAM Journal on Applied Mathematics*, 62(2):706–727.

Brown, T. G. (1911). The intrinsic factors in the act of progression in the mammal. *Proceedings of the Royal Society of London. Series B*, 84(572):308–319.

Clarke, J. D., Hayes, B. P., Hunt, S. P., and Roberts, A. (1984). Sensory physiology, anatomy and immunohistochemistry of Rohon-Beard neurones in embryos of *Xenopus laevis*. *The Journal of Physiology*, 348(1):511–525.

Donovan, M., Wenner, P., Chub, N., Tabak, J., and Rinzel, J. (1998). Mechanisms of spontaneous activity in the developing spinal cord and their

relevance to locomotion. *Annals of the New York Academy of Sciences*, 860(1):130–141.

Ermentrout, G. B. and Terman, D. H. (2010). *Mathematical foundations of neuroscience*, volume 35 of *Interdisciplinary Applied Mathematics*. Springer New York.

Fenichel, N. (1979). Geometric singular perturbation theory for ordinary differential equations. *Journal of Differential Equations*, 31(1):53–98.

Gaspard, P. and Wang, X. J. (1987). Homoclinic orbits and mixed-mode oscillations in far-from-equilibrium systems. *Journal of Statistical Physics*, 48(1-2):151–199.

Gavrilov, N. K. and Shilnikov, L. P. (1972). On three-dimensional dynamical systems close to systems with a structurally unstable homoclinic curve. I. *Mathematics of the USSR-Sbornik*, 17(4):467.

Kahn, J. A. and Roberts, A. (1982). The neuromuscular basis of rhythmic struggling movements in embryos of *Xenopus laevis*. *Journal of Experimental Biology*, 99(1):197–205.

Kahn, J. A., Roberts, A., and Kashin, S. (1982). The neuromuscular basis of swimming movements in embryos of the amphibian *Xenopus laevis*. *Journal of Experimental Biology*, 99(1):175–184.

Kuehn, C. (2015). *Multiple Time Scale Dynamics*, volume 191 of *Applied Mathematical Sciences*. Springer International Publishing.

Kuznetsov, A. (2004). *Elements of applied bifurcation theory*. Springer Science & Business Media.

Li, W.-C., Sautois, B., Roberts, A., and Soffe, S. R. (2007). Reconfiguration of a vertebrate motor network: specific neuron recruitment and context-dependent synaptic plasticity. *The Journal of Neuroscience*, 27(45):12267–12276.

Matveev, V., Bose, A., and Nadim, F. (2007). Capturing the bursting dynamics of a two-cell inhibitory network using a one-dimensional map. *Journal of Computational Neuroscience*, 23(2):169–187.

Morris, C. and Lecar, H. (1981). Voltage oscillations in the barnacle giant muscle fiber. *Biophysical Journal*, 35(1):193–213.

Nadim, F. and Manor, Y. (2000). The role of short-term synaptic dynamics in motor control. *Current Opinion in Neurobiology*, 10(6):683–690.

Nadim, F., Manor, Y., Kopell, N., and Marder, E. (1999). Synaptic depression creates a switch that controls the frequency of an oscillatory circuit. *Proceedings of the National Academy of Sciences*, 96(14):8206–8211.

Nelder, J. A. and Mead, R. (1965). A simplex method for function minimization. *The Computer Journal*, 7(4):308–313.

Press, W. H. (2007). *Numerical recipes 3rd edition: the art of scientific computing*. Cambridge University Press.

Rabbah, P. and Nadim, F. (2007). Distinct synaptic dynamics of heterogeneous pacemaker neurons in an oscillatory network. *Journal of neurophysiology*, 97(3):2239–2253.

Soffe, S. R. (1993). Two distinct rhythmic motor patterns are driven by common premotor and motor neurons in a simple vertebrate spinal cord. *The Journal of Neuroscience*, 13(10):4456–4469.

Tsodyks, M. V. and Markram, H. (1997). The neural code between neocortical pyramidal neurons depends on neurotransmitter release probability. *Proceedings of the National Academy of Sciences*, 94(2):719–723.